Journal of proteome research

Article

pubs.acs.org/jpr

Open Access on 03/06/2015

# Histone H1 Phosphorylation in Breast Cancer

Sean W. Harshman,[†,‡,¶] Michael E. Hoover,[†,‡,¶] Chengsi Huang,[§] Owen E. Branson,[§] Sarah B. Chaney,[⊥] Carolyn M. Cheney,[∥] Thomas J. Rosol,[⊥] Charles L. Shapiro,[‡] Vicki H. Wysocki,[§] Kay Huebner,[†,‡] and Michael A. Freitas*[,†,‡]

[†]Department of Molecular Virology, Immunology and Medical Genetics, [‡]Comprehensive Cancer Center, [§]Department of Chemistry & Biochemistry, [⊥]Veterinary Biosciences, College of Veterinary Medicine, and [∥]Department of Internal Medicine, Division of Hematology, The Ohio State University, Columbus, Ohio 43210, United States

Supporting Information

**ABSTRACT:** Breast cancer is the second leading cause of cancer-related deaths in women. The need for new clinical biomarkers in breast cancer is necessary to further predict prognosis and therapeutic response. In this article, the LC-MS histone H1 phosphorylation profiles were established for three distinct breast cancer cell lines. The results show that the extent of H1 phosphorylation can distinguish between the different cell lines. The histone H1 from the metastatic cell line, MDA-MB-231, was subjected to chemical derivitization and LC-MS/MS analysis. The results suggest that the phosphorylation at threonine 146 is found on both histone H1.2 and histone H1.4. Cell lines were then treated with an extracellular stimulus, estradiol or kinase inhibitor LY294002, to monitor changes in histone H1 phosphorylation. The data show that histone H1 phosphorylation can increase and decrease in response to extracellular stimuli. Finally, primary breast tissues were stained for the histone H1 phosphorylation at threonine 146. Variable staining patterns across tumor grades and subtypes were observed with pT146 labeling correlating with tumor grade. These results establish the potential for histone H1 phosphorylation at threonine 146 as a clinical biomarker in breast cancer.

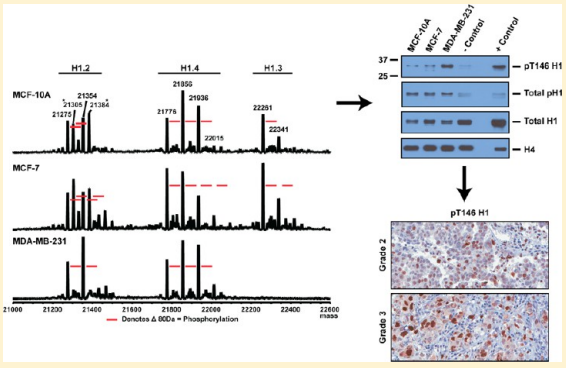


**KEYWORDS:** *histone H1, breast cancer, phosphorylation*

## INTRODUCTION

Breast cancer is the second leading cancer-related cause of mortality in women, accounting for more than 200 000 new cases and an estimated 40 000 deaths in 2010 alone.[1] Mammography is currently the leading clinical screening tool along with tissue biopsies for eventual diagnosis and staging. However, mammography has led to a greater number of false positives (>10%) and the potential for misdiagnosis and overtreatment.[2] Additionally, interpretation of tissue biopsies relies heavily on subjective identification of malignant cells within the tissue for diagnosis. Due to the nonspecific qualities of mammography and the imperfect nature of tissue biopsies, more sensitive tissue biomarkers for disease progression, metastases, and patient outcome are needed.

Global core histone modifications have been correlated with prognostic value in a host of cancer types including kidney, prostate, lung, pancreatic, and breast cancers.[3−6] While there is a deep knowledge of the core histones and their prognostic value in cancer, very little is known about the prognostic value of the linker histone H1. However, it has been established that antihistone H1 phospho antisera can be used in detecting invasive cancer.[7] Furthermore, such labeling has been shown to correlate with disease grade.[8] Thus, exploration of the usefulness of histone H1 phosphorylation to identify different cancer phenotypes remains uncertain and an area of research interest.

In this study, we examined the phosphorylation profiles and expression patterns of histone H1 in three distinct breast cancer cell lines and monitored their response to extracellular stimuli and therapeutic intervention. Next, we conducted LC-MS/MS analysis on purified histone H1 to identify the specific isoform(s) responsible for pT146 antisera labeling. Finally, we demonstrate immunohistochemical staining of pT146 in primary breast tumors across three tumor grades and four tumor subtypes. These data establish the potential use of histone H1 phosphorylation as a biomarker in breast cancer.

## EXPERIMENTAL PROCEDURES

### Antisera

Antisera used in this study were as follows. Primary antisera: phospho-T146 H1, total phospho-histone H1, total histone H1, total H4 (Abcam, Cambridge, MA), rabbit IgG from serum (BD Biosciences, San Jose, CA). Secondary antisera: anti-rabbit IgG/horseradish peroxidase (HRP), anti-mouse IgG-HRP (Cell

**Received:** December 16, 2013
**Published:** March 6, 2014

  

Signaling Technology, Inc., Danvers, MA), Alexa Fluor 488 anti-mouse, and Alexa Fluor 647 anti-rabbit (Invitrogen, Grand Island, NY). Dilutions, unless otherwise noted, were 1:1000 for primary and 1:3000 for secondary antisera.

### Cell Line Tissue Culture

Immortalized neoplastic MCF-7 and MDA-MB-231 as well as non-neoplastic MCF-10A cells were obtained from and cultured as recommended by American Type Culture Collection (Manassas, VA, USA). Briefly, all cells were maintained at approximately $5 \times 10^4$ cells/cm$^2$ by incubation at 37 °C with 5% $CO_2$. Culture medium was prepared as follows. MCF-7 modified from Soule et al.:[9] Dulbecco's modified Eagle medium (DMEM) media supplemented with 10% fetal bovine serum (FBS), 10 μg/mL recombinant human insulin (Sigma Aldrich, St. Louis, MO), 0.5 mg/mL L-glutamine (GlutaMAX), 50 U/mL penicillin-G, 50 μg/mL streptomycin (Pen/Strep), and 0.11 mg/mL sodium pyruvate (Life Technologies, Grand Island, NY). MDA-MB-231 modified from Fogh and Trempe:[10] DMEM supplemented with 10% FBS, L-glutamine, and Pen/Strep. MCF-10A modified from Soule et al.:[11] DMEM supplemented with 5% horse serum, 0.5 mg/mL hydroortisone, 10 ng/mL cholera toxin from *Vibrio cholerae*, 10 μg/mL recombinant human insulin (Sigma Aldrich, St. Louis, MO), 20 ng/mL recombinant human epidermal growth factor (Peprotech Inc., Rocky Hills, NJ), L-glutamine,and Pen/Strep. All media were filtered through a 0.22 μm membrane filter (Millipore, Billerica, MA). Asynchronous cells were harvested at approximately 50−70% confluency by collecting the media, washes, and trypsinized cells for histone extraction.

### Cell Synchronization

MDA-MB-231 cells were synchronized by double thymidine block.[12] Briefly, 100 mM thymidine (2 mM final dilution, Sigma Aldrich, St. Louis, MO) prepared in sterile PBS (Life Technologies, Grand Island, NY) was added for 18 h to cultures at approximately 25−30% confluency. Cells were washed twice with PBS and resuspended in fresh warmed culture medium for 9 h. A second thymidine block was performed, and cells were incubated for 16 h. Cells were washed and released from blocking as above. Aliquots were harvested at 0, 2, 4, 6, 8, and 12 h postrelease for histone extraction and flow cytometry.

### Hormone and Drug Exposures

MCF-7 cells were grown to approximately 30−50% confluency and treated with 70 nM estradiol (Sigma Aldrich, St. Louis, MO) or left untreated for 24 h. Cells were harvested postexposure for histone extraction and flow cytometry.

MDA-MB-231 cells were grown to 50−70% confluency and treated with DMSO (Sigma Aldrich, St. Louis, MO) and 5, 10, or 20 μM LY294002 (Biomol, Hamburg, Allemagne). Cells were harvested 24 h postexposure for histone extraction and flow cytometry.

### Chromosomal Spreading

MDA-MB-231 cells were grown to approximately 50−70% confluency and treated for 18 h with nocodazole (100 nM, Sigma Aldrich, St. Louis, MO). Cells were harvested, pelleted, and washed 1× with PBS. Five milliliters of prewarmed (37 °C) 75 mM potassium chloride (KCl, Fisher Scientific, Waltham, MA) was added dropwise to the cell pellets, and suspensions were left at 37 °C for 10 min. Aliquots (100 μL) of swelled cells were focused onto microscopy slides at 900 rpm for 10 min using a cytospin centrifuge (Shandon Cytospin 4, Thermo Electron, Waltham, MA). Focused cells were briefly dried, washed 4× with KCM buffer (120 mM KCl, 20 mM NaCl, 10 mM Tris-HCl pH 8.0, 0.5 mM EDTA, and 0.1% Triton X-100), fixed with 4% paraformaldehyde for 10 min at room temperature, rinsed 2× with KCM buffer, and blocked with 2% bovine serum albumin (BSA, Sigma Aldrich, St. Louis, MO) in KCM buffer for 1 h. Fixed cells were immunolabeled with primary antisera in 2% BSA overnight at 4 °C in a humidified chamber. Slides were washed 3× with 2% BSA/KCM buffer for 5 min with rocking. Secondary antisera labeling occurred for 1 h at room temperature in the dark. Fixed cells were washed again, mounted with DAPI mounting medium (Vectashield, Vector Laboratories Inc., Burlingame CA), cover-slipped, and stored at 4 °C in the dark until later use. Immunolabeling was repeated as needed for additional primary antisera. Chromosome spread images were obtained for confocal microscopy as described above.

### Histone Extraction

Histones were extracted from the chromatin of approximately $1 \times 10^8$ cells as described previously by Ren et al.[13] Briefly, pelleted cells were washed once with ice-cold PBS, placed in 1 mL of NP-40 extraction buffer (10 mM Tris-HCl pH 7.4, 10 mM NaCl, 3 mM $MgCl_2$, 0.5% NP-40, 0.15 mM Spermine, 0.5 mM Spermidine (aq)) supplemented with enzyme inhibitors (Sigma Protease Inhibitor Cocktail, 100 mM phenylmethyl sulfonyl fluoride, serine/threonine phosphatase inhibitor cocktail, tyrosine phosphatase inhibitor cocktail, Sigma Aldrich, St. Louis, MO), mixed, and allowed to stand on ice for 10 min. Nuclei were isolated at 200*g* for 10 min and washed with ice-cold PBS. Then, 400 μL of 0.4 N $H_2SO_4$ was added to the pelleted nuclei, and the mixture was allowed to stand for 30 min on ice. Nuclei suspensions were centrifuged at 21 000*g* for 10 min, and histones were precipitated from the supernatant at −20 °C overnight in ice-cold acetone. Histone precipitate was harvested by centrifugation at 21 000*g* for 10 min at 4 °C. Pellets were washed 1× with ice-cold acetone and centrifuged again. Histone precipitate was dissolved in HPLC water (J.T. Baker, Center Valley, PA) and stored at −80 °C until further use.

For LC-MS/MS analysis, histone H1s were enriched from MDA-MB-231 cells blocked for 18 h with nocodazole as previously described by Lindner et al.[14] Briefly, isolated nuclei were resuspended in a 5:1 final ratio 0.4 N $H_2SO_4$/cell pellet volume. Seventy percent $HClO_4$ was immediately added to a 10% final concentration. Solutions were allowed to stand for 45 min on ice. Histone H1 was precipitated from the supernatant as described above.

### Liquid Chromatography Mass Spectrometry (LC-MS)

Extracted histones were subjected to LC-MS analysis. HPLC separation was performed on a Dionex Ultimate 3000 HPLC (Dionex, Waltham, MA) directly connected to a MicroMass Q-TOF (MicroMass, Milford, MA) mass analyzer. Approximately 20 μg of extracted histones was separated on a 1.0 × 150 mm C18 column (Discovery Bio wide pore C18 column, 5 μm, 300 Å, Supelco, USA) using conditions described previously by Wang et al.[15] Briefly, mobile phase A was 0.05% TFA (Pierce, Rockford, IL) in HPLC water (J.T. Baker, Center Valley, PA), while mobile phase B was 0.05% TFA in acetonitrile (EMD Millipore, Billerica, MA). The gradient was increased linearly from 20% B to 30% B at 2 min, 35% B at 10 min, 50% B at 30 min, 60% at 35 min, and 95% at 36 min. The 95% B was held

for 4 min. Equilibration back to 20% B was conducted for 15 min.

During LC-MS analysis, the HPLC chromatograms are unable to distinguish between histone H1 variants and their phosphorylated species. As a result, the chromatographic peaks corresponding to histone H1 peaks were identified based on elution sequence.[16] The mass spectral data corresponding to histone H1 were analyzed by sequence mass identification, deconvolution (MaxEnt algorithm), and analysis using the MassLynx software 4.0 (Waters Corp., Milford, MA).

For LC-MS/MS analysis, perchloric acid extracted histone H1s were RP-HPLC purified under the conditions described above. Fractions corresponding to the histone H1 were collected and dried in a speedvac.

### Immunoblotting

Extracted histone protein concentrations were calculated by conducting a Bradford Assay (Bio-Rad, Richmond, CA).[17] Ten micrograms of extracted histones were loaded onto 15% SDS-PAGE gels, transferred to nitrocellulose, and blotted for pT146 of H1, total pH1, total H1, and H4 using HRP-conjugated secondary antisera and SuperSignal West Pico chemiluminescent substrate (Pierce, Waltham, MA).

### Histone H1 Tryptic Digestion and LC-MS/MS Sample Preparation

RP-HPLC purified histone H1 was resuspended in 100 mM ammonium bicarbonate buffer (Sigma Aldrich, St. Louis, MO) supplemented with 0.5% Rapigest surfactant (Waters Corp., Milford, MA) and 400 ng of trypsin (cleavage at K and R, Promega, Madison, WI). Solutions were placed at 37 °C overnight (>16 h) with light rocking. The digestion was quenched, and Rapigest was precipitated by the addition of formic acid (Acros, Geel Belgium) to 30% (v/v). Samples were incubated at 37 °C for 30 min and centrifuged at 21 000*g* for 10 min 3× to remove the Rapigest surfactant. Peptides in the supernatant were dried in a speedvac.

Dried H1 peptides were resuspended in 100 mM ammonium bicarbonate buffer, and concentrations were estimated using the 280 nm absorbance (NanoDrop ND-1000, NanoDrop, Wilmington, DE). Ten micrograms of peptides were subjected to lysine chemical derivitization as described by Garcia et al.[18] In short, monomethylated and unmodified lysine residues were converted to propionyl amides by reacting peptides with 25 μL of propionic anhydride (Sigma Aldrich, St. Louis, MO) mixed in 75 μL 2-propanol (J.T. Baker, Center Valley, PA) for 15 min at 37 °C. After each reaction, peptides were dried in a speedvac. This procedure was done twice to maximize lysine derivatization. H1 peptides were resuspended in an in-house preparation of 100 mM ammonium formate, and concentrations were approximated using a NanoDrop ND-1000 spectrometer.

Chemically derivatized peptides were also subjected to phosphopeptide enrichment using the Thermo Fe-NTA enrichment kit (Thermo, Waltham, MA). Enrichment was performed as outlined by the manufacturer.

### Fourier Transform LC-MS/MS and Database Search

Digested H1 peptides (300 fmol) were separated on a Waters 2D NanoACQUITY HPLC system (Milford, MA) directly coupled to a Thermo Scientific Orbitrap Elite mass analyzer (Waltham, MA). Simulated 1D runs were performed to accommodate the 2D setup of the LC system. Mobile phase solvents were (A1) 20 mM ammonium formate and (B1) acetonitrile for the first dimension and (A2) 0.1% formic acid (aq) and (B2) acetonitrile with 0.1% formic acid for the second dimension. Separations were conducted on a Waters NanoEase 300 μm × 50 mm, 5 μm, XBridge BEH130 C18 column for the first dimension and a Waters NanoACQUITY UPLC 75 μm × 150 mm, 1.8 μm, HSS T3 column for the second dimension. Each sample was injected onto the first dimension column and immediately eluted onto the trap column using 50% B1. Peptides were separated on the second dimension column at 35 °C under a linear gradient, starting at 5% B2 to 30% B2 over 55 min and 30% B2 to 40% B2 over 5 min with direct introduction into the mass analyzer.

The Orbitrap Elite MS was operated in FT/FT mode with the MS1 scan at a resolution of 240 000. Collision-induced dissociation (CID) was conducted in the LTQ MS, and protein fragments ($MS^N$) were detected in the Orbitrap Elite MS at a resolution of 30 000. Top five data-dependent mode was used with a dynamic exclusion of 3 s, a repeat count of 1, and an isolation width of 2.0 *m*/*z*. LC-MS/MS data were searched against both a Uniprot human histone H1 database (H1.0−H1.5, provided in Supplemental Data 1 in Supporting Information, 17May13) and a Uniprot complete human proteome (as of 18Sep12) using our in-house search engine MassMatrix (v 2.4.2). Search parameters included six trypsin-missed cleavages, MS1 mass tolerance of ±10 ppm, and an $MS^N$ mass tolerance of ±0.02 Da. The variable modifications searched were phosphorylation of Ser/Thr and propionylation of free lysine, monomethylated lysine, and N-terminal amine. False discovery was estimated using the reversed target database. Retention of positive protein identifications were based upon a 5% FDR and two unique peptide matches or two max decoys. All positive matches for phosphorylated histone H1 peptides were manually validated.

### Flow Cytometry

MDA-MB-231 and MCF-7 cells were subjected to cell cycle analysis monitoring DNA content by propidium iodide (PI) uptake as described by Whitfield et al.[19] Following treatment, cells were pelleted, washed with PBS, and fixed in 80% ethanol (aq) for 10 min. Samples were blocked with 2% BSA/PBS for 1 h, and the phospho-T146 primary antisera (prepared in 2% BSA/PBS) were added for 1 h at room temperature with gentle rocking. Pellets were washed several times with 2% BSA/PBS, and secondary antisera were added for 1 h at room temperature with gentle rocking in the dark. Pellets were washed again and stained for 30 min with PI staining solution (50 μg/mL propidium iodide, 10 mM Tris pH 7.5, 5 mM $MgCl_2$, 10 μg/mL DNase free RNase). All samples were stored in the dark for up to 24 h at 4 °C prior to analysis.

MDA-MB-231 cells were analyzed for viability staining using the LIVE/DEAD fixable near-IR dead cell stain kit 633 nm (Invitrogen, Grand Island, NY) per the manufacturer's recommendations. Briefly, following treatment, cells were washed with PBS and stained for 20 min at room temperature. Pellets were washed again and fixed with 1% paraformaldehyde for 10 min. Cells were washed and stored at 4 °C in the dark until analysis. All flow cytometry analyses were conducted on a Beckman Coulter FC500 and computationally analyzed using Kaluza Flow Analysis Software (Beckman Coulter, Brea, CA).

### Confocal Microscopy

MDA-MB-231 cells were grown on coverslips to approximately 50−70% confluency and treated with either nocodazole (100 nM) or left untreated. Cells were washed with PBS and fixed in 4% paraformaldehyde for 10 min. Coverslips were washed,

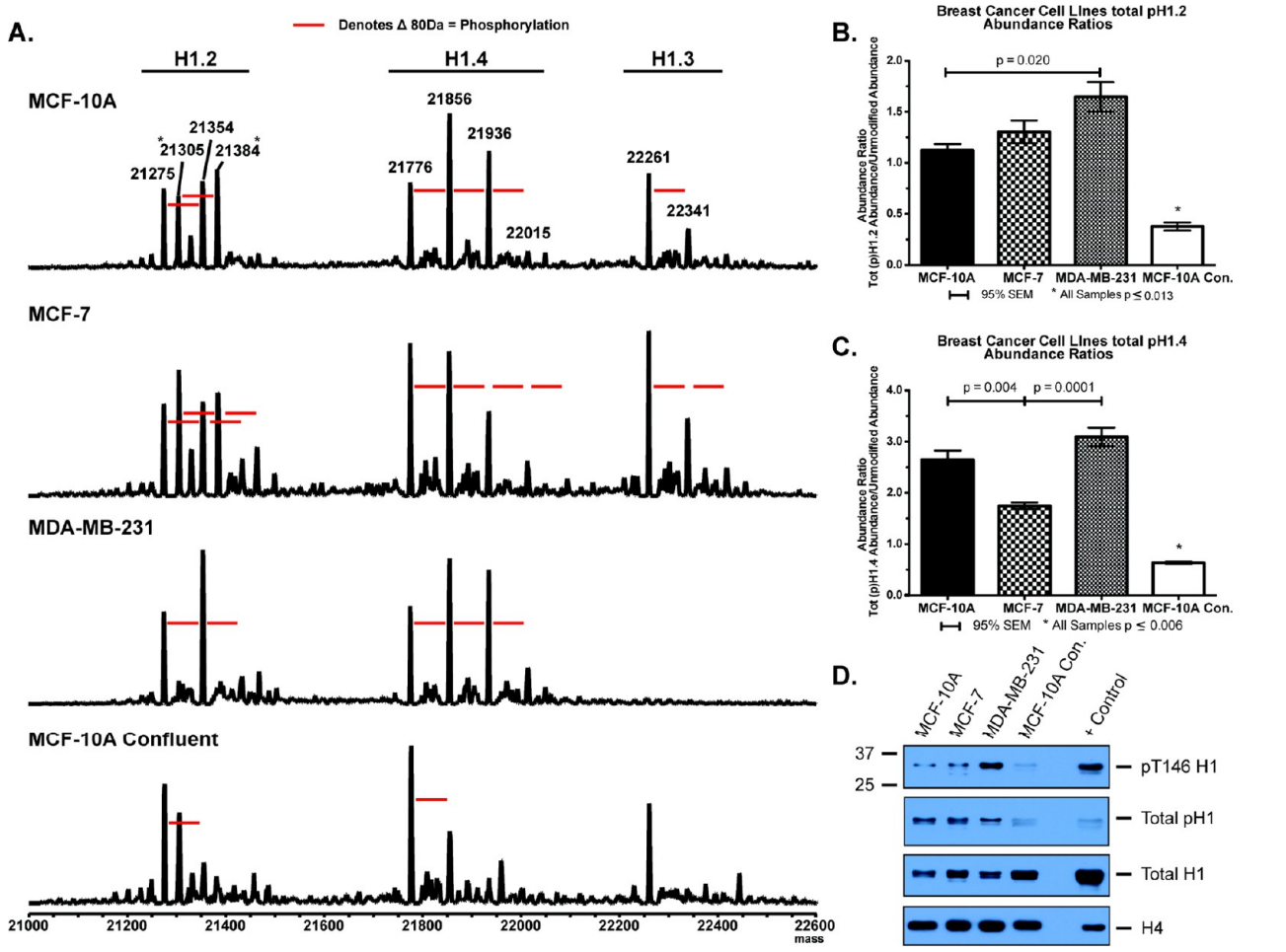


**Figure 1.** Asynchronous phosphorylation patterns of breast cancer cell lines by LC-MS and immunoblot. (A) Representative LC-MS spectra of acid extracted histones from the immortalized breast epithelial cell line, MCF-10A, and the neoplastic breast cancer cell lines, MCF-7 and MDA-MB-231. Bar chart of normalized abundance ratios from the LC-MS data for total phosphorylation of H1.2 (B) and H1.4 (C) from the breast cell lines. (D) Immunoblot of acid extracted histones from each breast cell line blotted for pT146 H1, total pH1, total H1, and H4 (loading control). Data show histone H1 has variable patterns of phosphorylation in asynchronous breast cells.

permeabilized with 0.1% Triton-X 100 for 5 min, washed again, and blocked for 1 h with 2% BSA/PBS. Primary antisera were added, and solution was allowed to stand overnight at 4 °C in a humidified chamber. Samples were washed with 2% BSA/PBS, and secondary antisera were allowed to stand overnight at 4 °C in a humidified chamber. Coverslips were washed, mounted with DAPI mounting media, and placed on slides for imaging. Slides were stored in the dark at 4 °C for no longer than 5 days before analysis. All images were obtained on an Olympus FV 1000 spectral confocal system (Olympus America, Center Valley, PA) under 40× and 100× objective lenses. Images were processed and combined using the Olympus FV 1000 Viewer software.

## Immunohistochemistry

Paraffin-embedded patient deidentified breast tissues were housed and obtained through The Ohio State Medical Center's Human Tissue Resource Network (HTRN). All tissues were stored, prepared, and immunohistochemically labeled by the HTRN core facility of The Ohio State University. Briefly, each tissue was cut at 4 $\mu$m and placed on positively charged slides. Slides were placed in a 60 °C oven for 1 h, cooled, deparaffinized, and rehydrated through xylene and graded ethanol solutions to water. All slides were quenched for 5 min in a 3% hydrogen peroxide solution in water to block for endogenous peroxidase. Heat-induced epitope retrieval was performed by placing the tissues in a 1× solution of target retrieval solution (Dako, Carpinteria, CA) for 25 min at 96 °C using a vegetable steamer (Black & Decker, New Britain, CT) and cooled for 15 min in solution. Slides were stained on a Dako Autostainer immunostaining system. The pT146 primary antisera were diluted (1:300) and incubated for 60 min. Tissues were blocked for endogenous biotin using the Dako biotin blocking system. Detection was performed using the Dako-labeled streptavidin−biotin−HRP complex and visualized using DAB chromogen (Dako). Tissues were counterstained in Richard Allen hematoxylin, dehydrated by graded ethanol solutions, and cover-slipped. Slides were scanned using Aperio ScanScope XT (Aperio, Vista, CA) at 20× magnification. Images were saved using the Aperio Image Scope Software.

## Pathological Evaluation

A total of 242 primary breast tissues and 97 normal nonbreast cancer tissues were immunohistochemically stained. Images of tissue staining can be found in Supplemental Data 10. Primary breast tissues were individually assessed for the pT146 percent total tumor staining and tumor stain intensity. Determinations for tumor staining and intensity were ranked based on a five-


dx.doi.org/10.1021/pr401248f | J. Proteome Res. 2014, 13, 2453−2467

point scale: rare or no staining (0), 4−25% (1), 26−50% (2), 51−75% (3), and 76−100% (4). Evaluation data are provided in Supplemental Data 11.

### Statistical Analysis

Bar charts for biological replicate LC-MS abundance ratios (total phosphorylation abundance/unmodified abundance) and LIVE/DEAD staining were generated using Prism GraphPad software (GraphPad Software Inc., La Jolla, CA). All statistical analyses were conducted using the *R* statistical analysis software.[20] For LC-MS data, ANOVA and Tukey tests were performed on abundance ratios to test for differences in the ratios of phosphorylation. For pathological data, a test for mutual independence was performed using the Pearson $\chi$-squared test across subtype, grade, and intensity of pT146 stain. Association plots for the ordered categorical data were generated using the vcd package.[21−23] Staining evaluations were grouped as ordered factors as follows: low stain (intensity of stain = 0, 1, or 2) and high stain (intensity of stain = 3 or 4). Grade values were grouped as the ordered factors low grade (grade = 1 or 2) and high grade (grade = 3 or 4) across all subtypes.

## RESULTS

### Histone H1 Phosphorylation Patterns in Breast Cancer Cell Lines

Liquid chromatography coupled with mass spectrometry has been successfully used to determine histone profiles.[16] Histone H1 variant expression and post-translational modifications have been shown, by LC-MS, to vary across cell type and cellular status.[15,24−26] A recent report has suggested histone H1 phosphorylation as a useful biomarker for labeling cancer cell proliferation.[8] To establish the expression patterns and post-translational modification profiles of histone H1 in breast cancer, we extracted histones from asynchronous breast cancer cell lines and subjected them to LC-MS analysis. Figure 1A depicts representative deconvoluted mass spectra of the histone H1 variants H1.2, H1.3, and H1.4 obtained from the three breast epithelial cell lines. The replicate spectra and total ion chromatograms are provided in Supplemental Data 2. The data in Figure 1A show variable patterns of histone H1 phosphorylation. For example, the neoplastic MCF-7 cell line has a greater number of histone H1.4 phosphorylations (denoted by an increased number of red bars) when compared to the number of phosphorylations on histone H1.4 of the immortalized breast epithelial cells MCF-10A and the metastatic breast cancer cell line MDA-MB-231. Similarly, both the neoplastic cell lines, MCF-7 and MDA-MB-231, have a greater number of histone H1.2 phosphorylations when compared to the immortalized breast epithelial, MCF-10A, cell line. Interestingly, the metastatic breast cancer cell line MDA-MB-231 has undetectable levels of both the histone H1.3 and H1.5 variants that were observed in the other two cell lines (Supplemental Data 2). Furthermore, both the MCF-10A and the MCF-7 cell lines express an allelic variant (A142T) of histone H1.2, denoted by a change in 30 Da, observed previously in HeLa cells by Zheng et al. and in Ramos cells by our group.[25,26]

The normalized abundance ratios (total phosphorylated peak abundance/unmodified peak abundance) for both H1.2 and H1.4 were calculated across each replicate injection and are shown in Figures 1B,C. Histones H1.3 and H1.5 were not included in this analysis, as they were not detected in any of the MDA-MB-231 injections (Supplemental Data 2). For individual replicate peak abundances and ratio calculations, see Supplemental Data 3. These data illustrate the differences in the abundance of the H1.2 and H1.4 phosphorylation states across the three breast epithelial cell lines. For instance, Figure 1B shows a statistically significant increase in the total abundance of the H1.2 phosphorylation between the immortalized breast epithelial cells, MCF-10A, and the metastatic breast cancer cell line, MDA-MB-231. Furthermore, total histone H1.4 phosphorylation is reduced in the neoplastic MCF-7 cell line when compared to the MCF-10A and MDA-MB-231 cell lines, although the number of phosphorylations on the H1.4 of MCF-7 cells is increased (Figure 1A,C). Collectively, these data show differences in histone H1 phosphorylation across these breast cancer cell lines.

The commercially available polyclonal antisera against threonine 146 phosphorylation (pT146) on the variants H1.2, H1.3, and H1.4 were used to monitor H1 phosphorylation across these breast cell lines. While these antisera have been previously used in biochemical assays, they cannot distinguish between the three H1 variants due to sequence homology.[8,24] Immunoblotting with the antisera reveals a higher level of pT146 in the metastatic breast cancer cell line MDA-MB-231 when compared to the MCF-10A and MCF-7 cell lines (Figure 1D). Since the LC-MS data presented in Figure 1A and Supplemental Data 2 show that MDA-MB-231 cells have undetectable levels of histone H1.3, these results suggest that phosphorylation of histone H1 at T146 in MDA-MB-231 cells is independent of H1.3. Additionally, the signal intensity observed in the blots shown in Figure 1D for pT146 phosphorylation follows the pattern of pT146 phosphorylation quantified in Figure 1A. Collectively, these data confirm that phosphorylation profiles of histone H1 are variable across these breast epithelial cell lines. Additionally, the results indicate that H1 phosphorylation profiles have potential to distinguish between these breast cancer cell types.

### LC-MS/MS Analysis of Histone H1 from MDA-MB-231 Cells

The commercially available antisera against H1 T146 phosphorylation are expected, due to sequence homology, to label multiple H1 isoforms (H1.2, H1.3, and H1.4). Identification of the specific H1 isoform(s) responsible for pT146 labeling will allow for a better understanding of both the in vitro and in vivo results obtained with this antiserum. Using MDA-MB-231 cells arrested in mitosis as an in vitro model for high T146 phosphorylation, we performed LC-MS/MS analysis to determine the specific isoform(s) associated with this modification.

The in silico tryptic digest of H1.2 and H1.4 shows that the peptides encompassing the T146 residue contain different amino acid sequences. However, the extensive lysine content in the C-terminal domain of H1 results in extremely hydrophilic tryptic peptides.[27] For reversed-phase HPLC separation, it is necessary to increase the hydrophobic nature of these peptides to facilitate separation. Several reports have identified the use of lysine chemical derivitization by propionic anhydride to bind free and monomethylated lysine, thereby increasing the hydrophobicity of hydrophilic peptides.[18,28,29] Using a modified version of the method originally described by Garcia et al., we obtained adequate separation of the hydrophilic H1 peptides across a 1 h HPLC gradient for both shotgun and phosphopeptide enriched samples (Supplemental Data 4).[18] Database searches of the FT/FT LC-MS/MS data against both

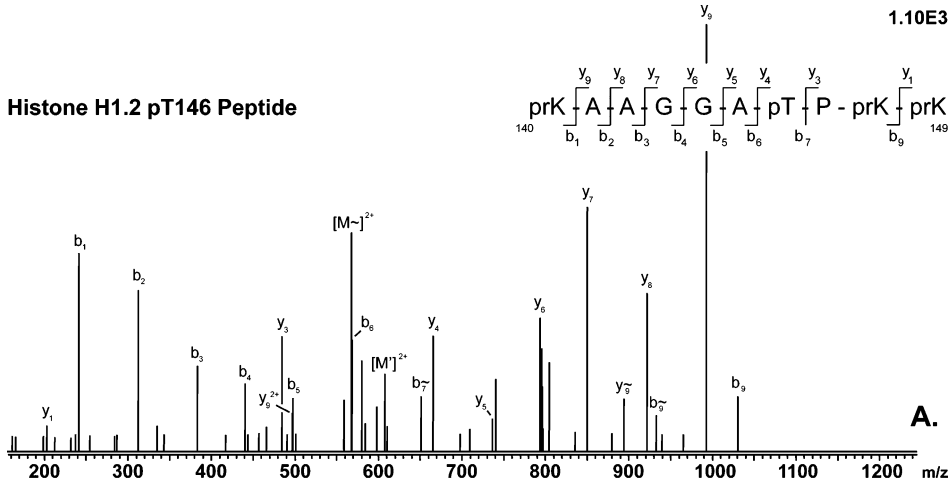


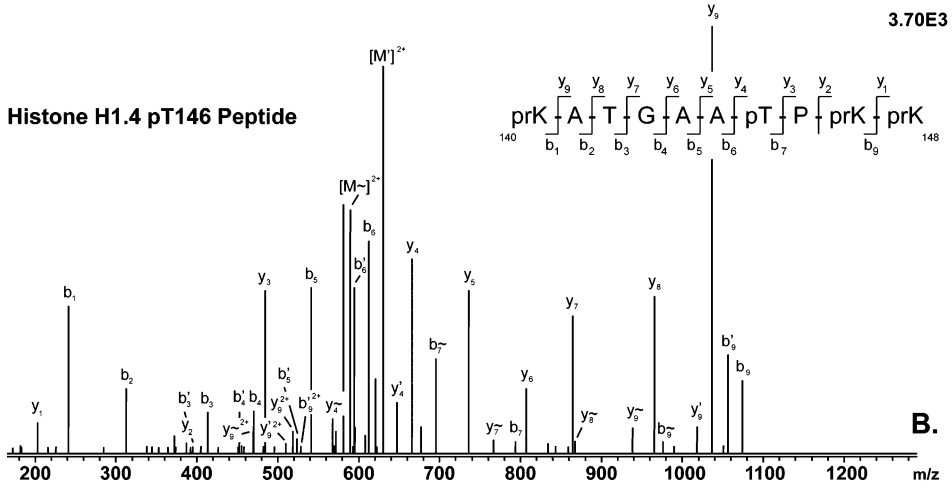


| H1 Isoform | Amino Acids | Sequence | Phosphorylation Site | Method |
|---|---|---|---|---|
| H1.2 | 140 - 148 | KAAGGATPK | T146 | PPE |
| | 140 - 149 | KAAGGATPKK | T146 | PPE |
| | 149 - 156 | KSAKKTPK | T154 | PPE |
| | 150 - 156 | SAKKTPK | T154 | SP, PPE |
| | 169 - 175 | KVAKSPK | S173 | SP, PPE |
| | 169 - 176 | KVAKSPKK | S173 | PPE |
| | 170 - 175 | VAKSPK | S173 | PPE |
| H1.4 | 26 - 32 | KSAGAAK | S27 | PPE |
| | 140 - 148 | KATGAATPK | T146 | SP, PPE |
| | 140 - 149 | KATGAATPKK | T146 | SP, PPE |
| | 149 - 156 | KSAKKTPK | T154 | PPE |
| | 150 - 156 | SAKKTPK | T154 | SP, PPE |
| | 169 - 174 | KAKSPK | S172 | SP, PPE |
| | 169 - 175 | KAKSPKK | S172 | SP, PPE |
| | 183 - 190 | KAPKSPAK | S187 | SP, PPE |

C.

**Figure 2.** LC-MS/MS spectra of propionylated histone H1 trypsin digests from MDA-MB-231 cells. (A) MS/MS spectra for the phosphorylated T146 peptide of H1.2. (B) MS/MS spectra for the phosphorylated T146 peptide of H1.4. (C) List of additional CDK phosphorylation sites identified on mitotic histone H1 in MDA-MB-231 cells: pr = propionylation, p = phosphorylation, ′ = loss of $H_2O$, ∼ = loss $HPO_3$, SP = shotgun proteomics, and PPE = phospho peptide enrichment. Results suggest pT146 phosphorylation occurs on both H1.2 and H1.4 in MDA-MB-231 cells.

the Uniprot human histone H1 and Uniprot complete human proteome databases showed identification of the pT146 peptide from both the H1.2 and H1.4 isoforms using the phospho peptide enrichment kit (Figure 2A,B). However, only the H1.4 pT146 peptide was identified in the shotgun proteomic H1 sample (Figure 2C). These results suggest the epitope labeled by the pT146 antisera is present on both H1.2 and H1.4 in the MDA-MB-231 cell line.

During mitosis, histone H1 has been shown to have maximal phosphorylation.[30−36] To identify if our methodology is able to detect additional phosphorylation sites, we expanded database searches of the FT/FT LC-MS/MS data for other sites of H1 phosphorylation. Both phosphopeptide enrichment and shotgun proteomic strategies for histone H1 were able to identify several other histone H1.2 and H1.4 phosphorylation sites (Figure 2C). The identification of pT154 and pS173 on H1.2 and pS27, pT154, pS172, and pS187 on H1.4 by mass spectrometry is supported by several other studies (Supplemental Data 5).[24,37−40] Every phosphorylation site identified in this study has been previously characterized as consensus


dx.doi.org/10.1021/pr401248f | J. Proteome Res. 2014, 13, 2453−2467

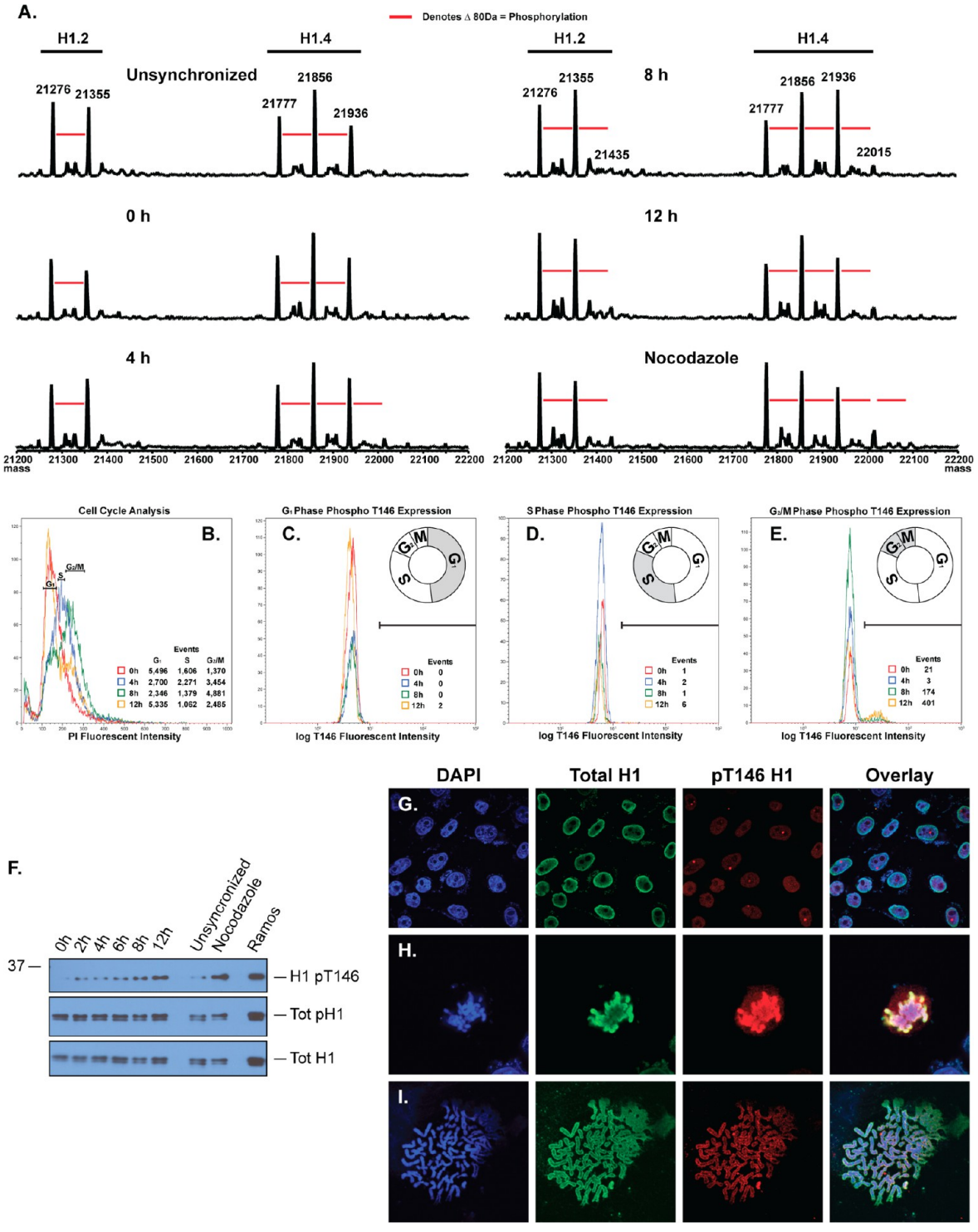


**Figure 3.** Cell cycle analysis utilizing MDA-MB-231 cells for phospho histone H1 analysis. (A) LC-MS spectra of histone H1 extracted from synchronized and asynchronous MDA-MB-231 cells. (B) Cell cycle analysis by flow cytometry of DNA content by propidium iodide uptake. (C) pT146 content in the $G_1$ phase of the cell cycle. (D) pT146 content in the S phase of the cell cycle. (E) pT146 content in the $G_2$/M phase of the cell cycle. (F) Immunoblot for pT146 expression across time points of the cell cycle. (G) Immunofluorescence of pT146 staining of interphase MDA-MB-231 cells. (H) Immunofluorescence of pT146 staining of a mitotic MDA-MB-231 cell. (I) Immunofluorescence of pT146 staining from metaphase chromosomal spreads. Data show that pT146 is primarily a mitotic phosphorylation site.

cyclin-dependent kinase (CDK) sites with the phosphorylation occurring at (S/T)PXK sequences.[27] However, not all the consensus CDK sites were identified in our samples. Phosphorylation at T31 of H1.2 and T18 of H1.4 was not detected, although described as consensus CDK sites.[27] These data suggest that T31 and T18 phosphorylation on H1.2 and H1.4 is absent or below the limit of detection for the assay.

While these additional sites of H1 phosphorylation were identified in the MS/MS data, quality specific antisera against such H1 post-translational modifications are drastically


dx.doi.org/10.1021/pr401248f | J. Proteome Res. 2014, 13, 2453−2467

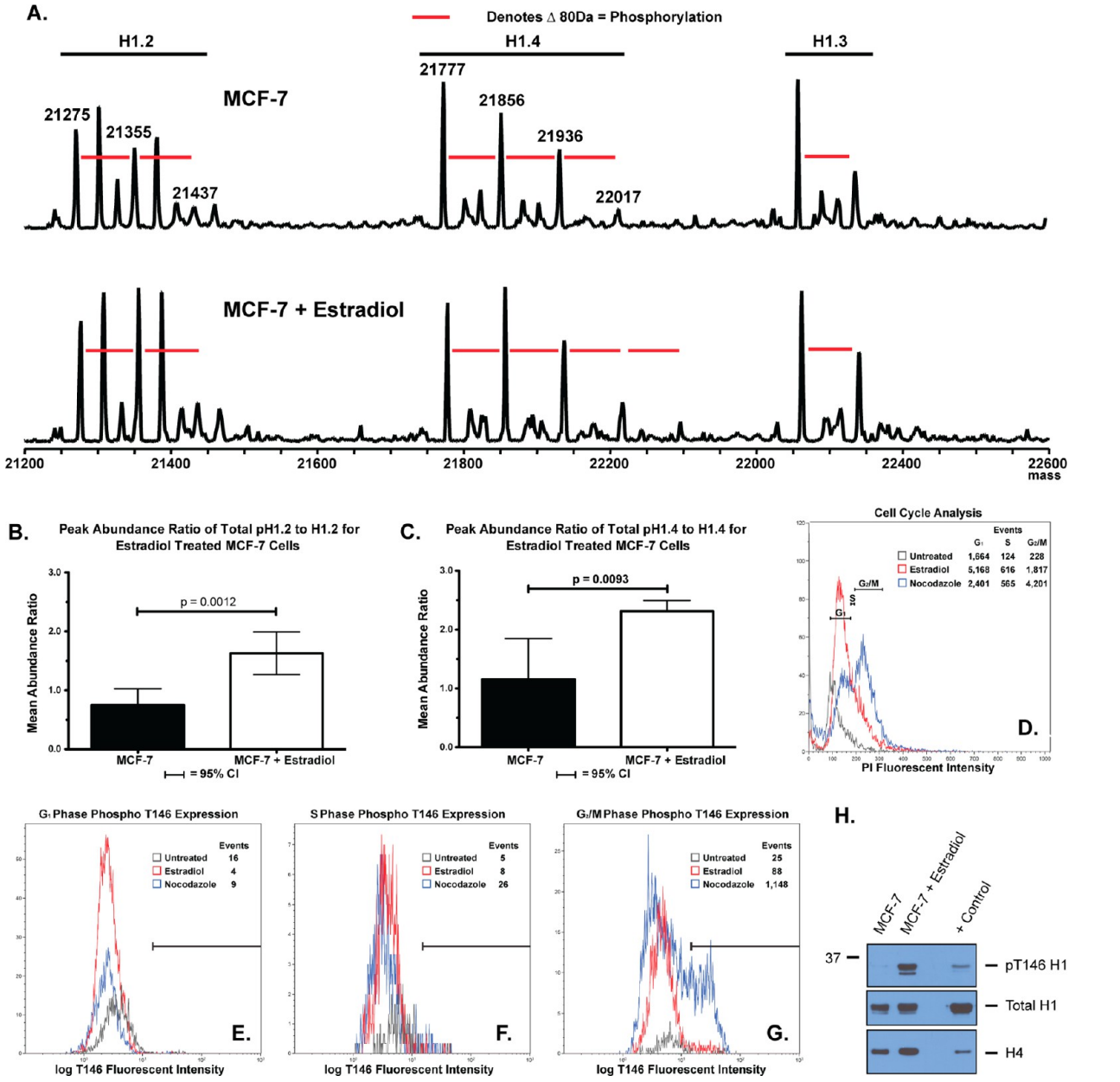


**Figure 4.** Phosphorylation of MCF-7 cells in response to estradiol stimuli. (A) LC-MS spectra of histone H1 isolated from untreated MCF-7 cells or those treated with 70 nM estradiol for 24 h. Bar chart of mean normalized abundance ratios of the LC-MS data for total phosphorylation of H1.2 (B) and H1.4 (C) from the treated or untreated MCF-7 cells. (D) Cell cycle analysis via PI uptake for DNA content of MCF-7 cells treated with estradiol. (E) pT146 content in the $G_1$ phase of the cell cycle. (F) pT146 content in the S phase of the cell cycle. (G) pT146 content in the $G_2$/M phase of the cell cycle. (H) Immunoblot for pT146 in response to estradiol exposure. Data show that MCF-7 cells treated with estradiol show increased pT146 H1 phosphorylation.

lacking.[27] Therefore, reliable confirmation of their presence by immunoblot cannot be performed. For this reason, this article focuses on T146 phosphorylation rather than other sites of H1 post-translational modification.

## Characterization of H1 Phosphorylation Across the Cell Cycle

The LC-MS/MS experiment identified several potential histone phosphorylation sites in the MDA-MB-231 cells for further investigation (Figure 2 and Supplemental Data 5). Of these sites, the pT146 antisera are commercially available and validated for many applications.[8,24,25,41,42] Therefore, the pT146 site on histone H1 was selected for further validation in breast cancer. Phosphorylation of histone H1 has been shown to progressively increase as cells advance through the cell cycle.[30−36] Although others have described specific histone H1 phosphorylation sites as interphase and/or mitotic through blocking experiments, we sought to monitor the specific phosphorylation site pT146 on histone H1 across the entire cell cycle.[24,25,41,42] Using MDA-MB-231 cells as a model cell line due to the high histone H1 phosphorylation content (Figure 1), we conducted cell synchronization experiments as originally described by Bostock et al. to monitor H1 phosphorylation.[12] Figure 3B shows the change in DNA content by detecting propidium iodide fluorescent intensity using flow cytometry following cell synchronization. These results show by 8−12 h nearly all the cells have reached mitosis. Figure 3A shows the


dx.doi.org/10.1021/pr401248f | J. Proteome Res. 2014, 13, 2453−2467

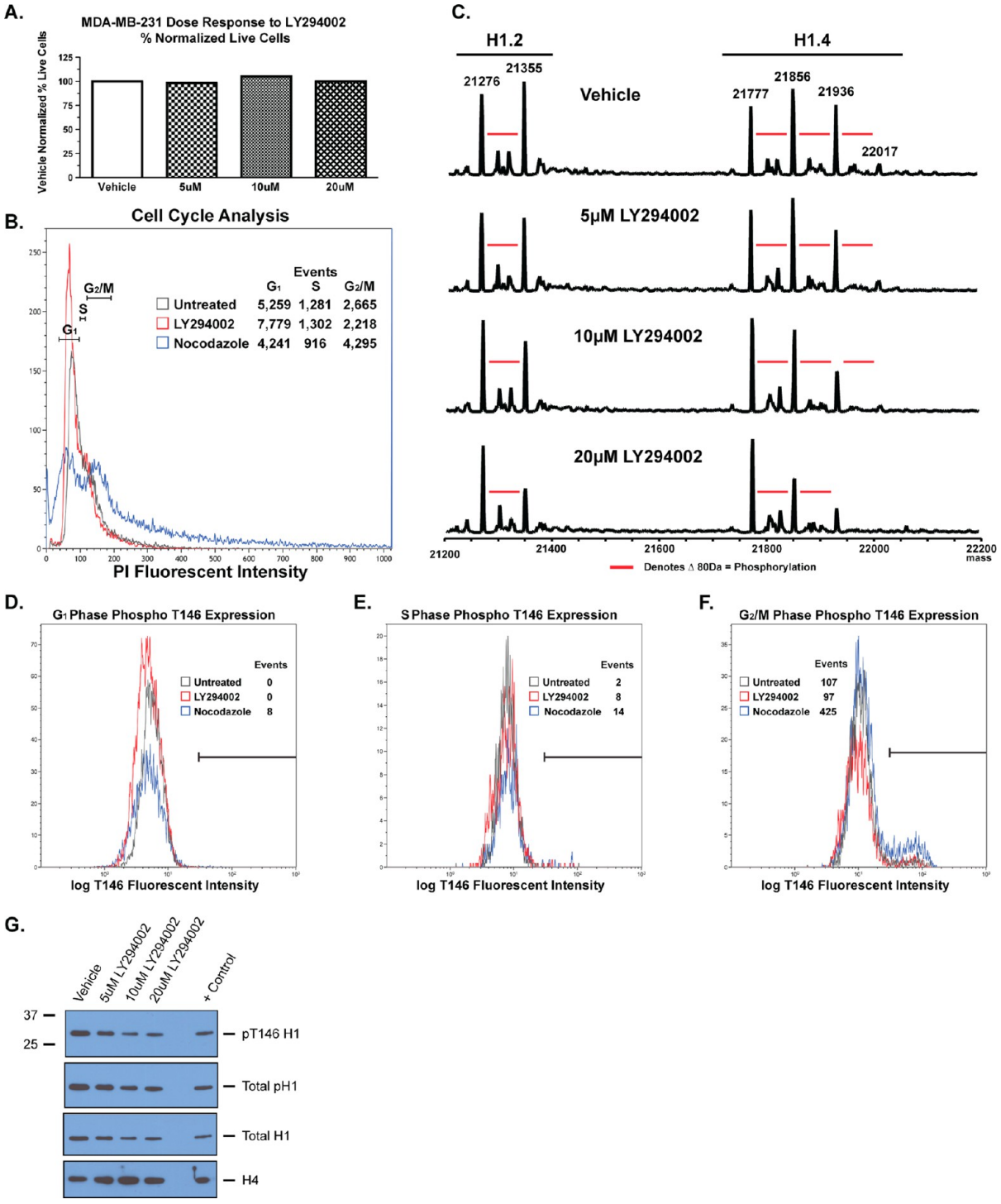


**Figure 5.** Phosphorylation of MDA-MB-231 cells in response to kinase inhibitor treatment, LY294002. (A) LIVE/DEAD staining of MDA-MB-231 cells by flow cytometry following kinase inhibitor treatment. (B) Cell cycle analysis via PI staining for DNA content of MDA-MB-231 cells treated with 10 $\mu$M kinase inhibitor treatment. (C) LC-MS spectra of histone H1 extracted from kinase inhibitor treated MDA-MB-231 cells. (D) pT146 content in the $G_1$ phase of the cell cycle. (E) pT146 content in the S phase of the cell cycle. (F) pT146 content in the $G_2$/M phase of the cell cycle. (G) Immunoblot for pT146 content in response to kinase inhibitor treatment. Data show a decrease in phospho-146 of H1 in response to kinase inhibitor therapy.

deconvoluted LC-MS spectra of the linker histones extracted from the synchronized MDA-MB-231 cells across five points in the cell cycle. See Supplemental Data 6 for the total ion chromatograms from each LC-MS analysis. These data show that H1 phosphorylation increases as cells progress through the cell cycle. The results from these LC-MS experiments are supported by various other studies that have examined the cell cycle dependence of H1 phosphorylation.[30−36]

Although others have described sites of histone H1 phosphorylation as interphase or mitotic, we assessed the specific phosphorylation site pT146 throughout the cell cycle. To do so, gates were fixed on the $1n$ ($G_1$), $1 - 2n$ (S), or $2n$


dx.doi.org/10.1021/pr401248f | J. Proteome Res. 2014, 13, 2453−2467

($G_2$/M) populations of DNA content from Figure 3B. The log pT146 fluorescent intensity associated with each of these gates was determined, and histograms for these data are shown in Figure 3C−E. These results reveal that pT146 staining is primarily found in the $G_2$/M phase of the cell cycle (Figure 3E). Furthermore, an immunoblot was conducted on extracted histones from each time point. Figure 3F shows an increase in the pT146 content at the 8−12 h ($G_2$/M) time points. These data are further supported by confocal immunofluorescence experiments on both interphase and mitotic cells. The images in Figure 3G depict DAPI (DNA stain), total H1, and pT146 staining of interphase MDA-MB-231 cells. These images show a small amount of focused pT146 nuclear staining. Conversely, using similar immunostaining methods on metaphase (mitotic) MDA-MB-231 cells, we observe a large amount of pT146 staining on the condensed chromatin (Figure 3H). Furthermore, chromosomal spreading experiments of nocodazole blocked cells show a uniform staining of pT146 across all condensed chromosomes (Figure 3I). These results are supported by other studies that suggest threonine and, more specifically, pT146 phosphorylation occurs during mitosis.[24,25,41,42] Additionally, the immunofluorescence and immunoblot data presented in Figure 3F,G suggest a small amount of interphase pT146 may also exist.

## Histone H1 Phosphorylation in Response to Estradiol in Vitro

A hallmark prognostic indicator of patient survival and predictive measure of therapeutic response in breast cancer is the expression of the estrogen receptor (ER) by breast tumor cells.[43] Signaling through the ER has been shown to increase proliferation of ER positive cells lending to increased tumor burden.[44] However, patients with estrogen receptor positive tumors generally respond therapeutically to estrogen receptor signaling inhibitors such as Nolvadex (tamoxifen) leading to increased overall survival.[43] In an in vitro setting, ER positive MCF-7 cells have long been used to investigate pathways associated with estrogen stimulation and growth.[45−47]

To define the changes in histone H1 phosphorylation in response to estrogen stimulation, we treated MCF-7 cells with 70 nM estradiol and conducted LC-MS on the extracted histones following treatment. Figure 4A depicts representative deconvoluted spectra from the 24 h estradiol stimulated and unstimulated cells. Total ion chromatograms and replicate spectra can be found in Supplemental Data 7. These data show an increase in number of histone H1 phosphorylations detected (denoted by an increase in the number of red lines) in response to estradiol when compared to the untreated MCF-7 cells. Similarly, the abundance ratios calculated for total H1.2 and H1.4 phosphorylation are significantly increased by estradiol stimulation (Figure 4B,C and Supplemental Data 8). To further elucidate the events surrounding histone H1 phosphorylation and estradiol stimulation, we conducted a cell cycle analysis by flow cytometry for DNA content on the hormone treated MCF-7 cells. The data presented in Figure 4D show estradiol stimulation causes an increase in the number of MCF-7 cells in the $G_2$/M stage of the cell cycle when compared to the untreated population. Furthermore, when gating on the cell cycle stage, data show that pT146 staining is again localized to the $G_2$/M phase of the cell cycle, with estradiol stimulation increasing the staining (Figure 4E−G). The LC-MS and flow cytometry results were confirmed by the immunoblot for pT146 seen in Figure 4H. The blot in Figure 4H shows a large increase in T146 phosphorylation on histone H1 when cells are treated with estradiol. Collectively, these data suggest that extracellular stimuli such as estradiol can modulate the histone H1 phosphorylation profiles in a disease-relevant in vitro system. Furthermore, the results presented in Figure 4 support the use of histone H1 phosphorylation at T146 as a biomarker for mitotic index.[7,8]

## Histone H1 Phosphorylation in Response to Kinase Inhibitor Therapy

Kinase inhibitors have become attractive antineoplastic agents due to the aberrant activation of many cellular kinases in numerous cancers and their potential for targeted therapy.[48] Unregulated, or constitutive, kinase activity has been shown to lead to increased tumor cell survival and drug resistance both in vitro and in vivo.[48] One such kinase, phosphatidylinositol 3-kinase (PI3K), is unregulated in a number of malignancies including breast cancer.[48] Utilizing the PI3K-dependent MDA-MB-231 breast cancer cell line as an in vitro model, we sought to monitor changes in histone H1 phosphorylation in response to kinase inhibitor therapy.

MDA-MB-231 breast cancer cells were treated in vitro with varying doses of the pan PI3K inhibitor, LY294002, for 24 h. LY294002 has been previously shown to cause growth inhibition and decreased motility in in vitro breast cancer models, such as MDA-MB-231 cells.[8,49,50] To establish that the kinase inhibitor therapy did not decrease viability of the treated cells (thus changing phosphorylation due to dead cell populations), LIVE/DEAD staining by flow cytometry was performed. Figure 5A shows the vehicle normalized % live MDA-MB-231 cells following LY294002 treatment. Similarly, Figure 5B shows the cell cycle analysis by propidium iodide uptake of MDA-MB-231 treated with 10 $\mu$M LY294002 or left untreated for 24 h. These data show that LY294002 treatment of MDA-MB-231 cells across three doses did not decrease the viability compared to the vehicle treatment. Additionally, the cell cycle analysis shows that LY294002 causes MDA-MB-231 cells to arrest in the $G_1$ phase of the cell cycle.

To assess the change in total histone H1 phosphorylation in response to different doses of LY294002, we performed LC-MS on the histones isolated from these cells. Figure 5C shows the deconvoluted spectra for histones H1.2 and H1.4 isolated from treated MDA-MB-231 cells. See Supplemental Data 9 for the total ion chromatograms from each LC-MS injection. As expected, the LC-MS data depict a dose-dependent reduction in H1.2 and H1.4 phosphorylation in response to the LY294002 drug treatments (Figure 5C). Additionally, the pT146 phosphorylation was monitored across the different phases of cell cycle by flow cytometry (Figure 5D−F). These results show that the pT146 staining in the $G_2$/M phase of the cell cycle is reduced with LY294002 treatment. The immunoblot conducted on histones isolated from the drug treated cells in Figure 5G illustrates a dose-dependent reduction in pT146 on histone H1 across the three drug concentrations. These data show the reduction in the global histone H1 phosphorylation, and specifically the T146 phosphorylation, by LC-MS, flow cytometry, and immunoblot as a result of LY294002 exposure. Collectively, these data illustrate the utility for histone H1 phosphorylation, particularly at the T146 site, for monitoring therapeutic response.

## Histone H1 Phosphorylation in Primary Breast Tumors

A recent report established that staining of histone H1 phosphorylation at T146 in bladder cancer tumor tissue can

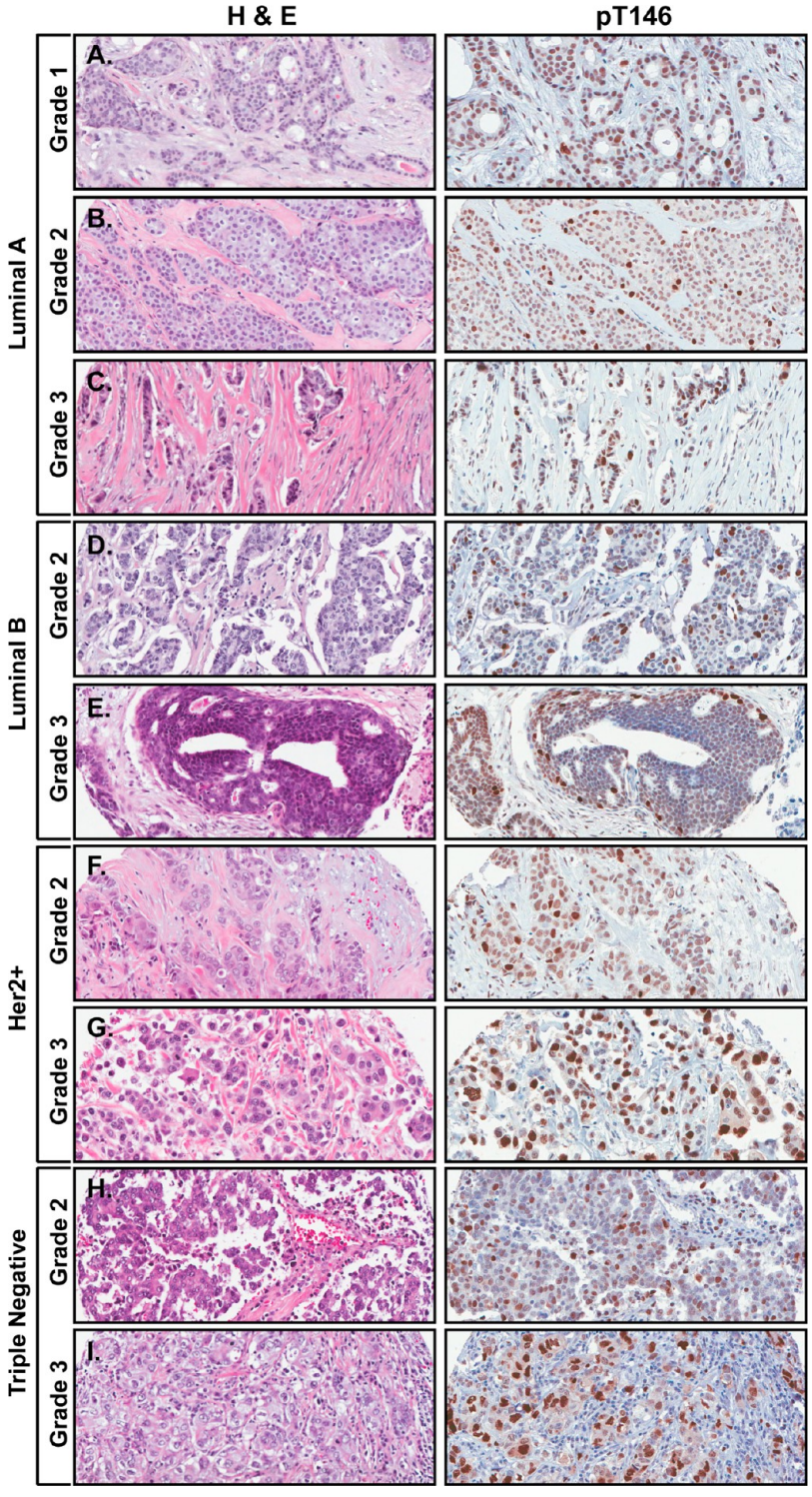


**Figure 6.** Immunohistochemical staining of primary breast tumors for Hematoxylin, eosin (H&E) and pT146: (A) grade I Luminal A, (B) grade II Luminal A, (C) grade III Luminal A, (D) grade II Luminal B, (E) grade III Luminal B, (F) grade II Her2, (G) grade III Her2, (H) grade II triple negative, (I) grade III triple negative. Data show specific staining patterns based upon grade and tissue subtype.

correlate with tumor grade.[8] To establish the histone H1 pT146 staining patterns and proof of principle in vivo, we immunohistochemically stained 242 primary tumor tissues taken from breast cancer patients with carcinoma representing three tumor grades. Additionally, 97 nonbreast cancer tissues were stained for reference (Supplemental Data 10). Grade I tumor tissues are classified as well-differentiated, grades II as intermediate, and grade III+ as poorly differentiated tissue. Figure 6A–C shows both the hematoxylin and eosin (H&E) and pT146 staining patterns across three grades of Luminal A (estrogen receptor (ER)/progesterone receptor (PR) positive, human epithelial growth factor receptor (Her2) negative) primary tumors. The grade I tumor shows diffuse low intensity staining in the nuclei of tumor cells about the mammary ducts when stained for pT146 (Figure 6A). The grade II Luminal A tissues contain an overall light speckled staining of the nuclei of


dx.doi.org/10.1021/pr401248f | J. Proteome Res. 2014, 13, 2453–2467

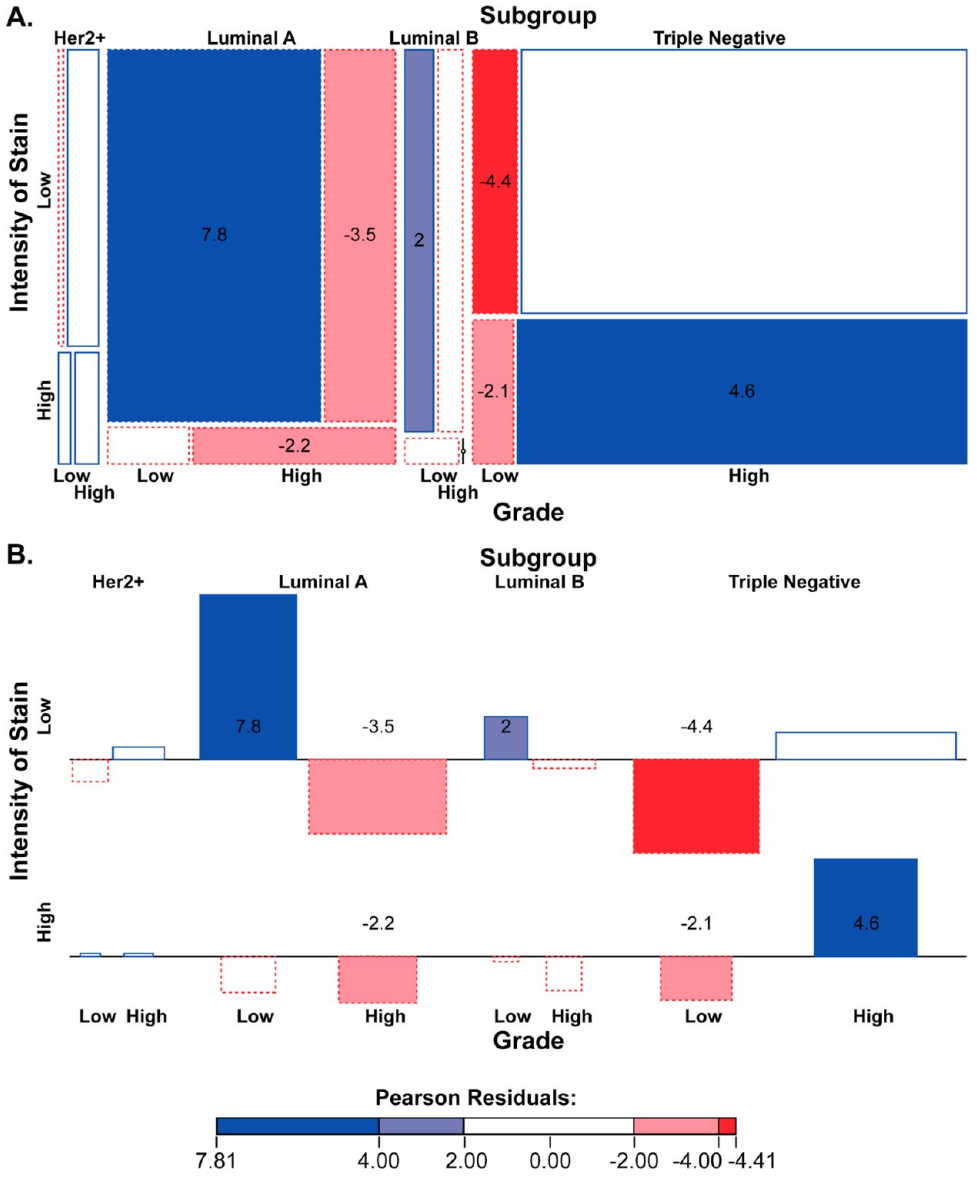


**Figure 7.** Statistical analysis of pT146 immunohistochemical staining in primary breast tumors. (A) Mosaic plot of stain intensity by grade and tumor subtype. (B) Association plot of stain intensity by grade and tumor subtype. Data show a significant association between pT146 staining and tumor grade.

tumor cells with individual very intense stained nuclei scattered throughout the tissue (Figure 6B). The grade III tissues show a large number of clustered and individual cells with intense nuclear pT146 staining (Figure 6C). The data show specific staining patterns across the three Luminal A breast tumor grades.

While Luminal A is the most common breast tumor subtype, three other tumor subtypes exist: Luminal B (ER/PR/Her2 positive), Her2+ (ER/PR negative, Her2 positive), and triple negative (ER/PR/Her2 negative). Patients with these tumor subtypes have variable expression of the three common proteins exploited for targeted therapeutics and as a result have a poorer prognosis and shorter overall survival than those with Luminal A tumors.[51,52] To establish the pT146 staining patterns in these tumor subtypes, we immunohistochemically stained Luminal B, Her2+, and triple negative tumors (Figure 6D–I). The pT146 staining in the low-grade tumors of Luminal B (Figure 6D), Her2+ (Figure 6F), and triple negative (Figure 6H) shows moderate diffuse speckled staining with a large number of cells displaying intense nuclear stain. Conversely, the high-grade tumors from the Luminal B (Figure 6E), Her2+ (Figure 6G), and triple negative (Figure 6I) have the most intense pT146 stain with a majority of the tumor cells displaying this phenotype. Collectively, the results suggest that staining patterns of pT146 on histone H1 may have clinical utility to discern tumor grade across breast tumor subtypes as has been shown in bladder cancer.[8]

To quantitatively assess the pT146 staining patterns in breast cancer primary tissues, each tumor was pathologically assessed for intensity and amount of pT146 stain in the cancer cells of each tissue. The results of the pathological evaluation, clinical biomarker data, and thumbnail images of each tumor microarray are provided in Supplemental Data 10, 11, and 12. A Pearson $\chi$-squared test for independence was then used to test for associations across pT146 stain intensity, tumor grade, and tumor subtype. A test for mutual independence yielded a $p$ value $<2.2 \times 10^{-16}$, suggesting a strong interdependence between stain, grade, and tumor subtype.


dx.doi.org/10.1021/pr401248f | J. Proteome Res. 2014, 13, 2453–2467

Figure 7A,B shows the mosaic and association plots for pT146 stain intensity, tumor grade, and subtype. The data show a significant association (denoted in blue or red) between the pT146 staining intensity and high-grade triple negative breast cancer tumors (i.e., staining intensity increases as tumor grade increases). Similarly, the Luminal A subtype shows a strong association between low intensity staining and low-grade tumors. Due to the limited number of samples in this data set, confident associations are difficult to assess for the Her2+ and Luminal B subtypes. Associations were also observed across tumor grade and subtype. The data presented would benefit from additional tumors from the under represented categories, such as high-grade Luminal A, low-grade triple negative, and all grades of Luminal B and Her2+. However, work to collect and obtain such tumor biopsies has proven to be difficult. Collectively, these results suggest that the intensity of pT146 stain can distinguish low- and high-grade tumors of the breast as has been shown for bladder.[8]

## DISCUSSION

Breast cancer is a leading cause of malignant mortality and morbidity in women worldwide.[1] The use of traditional biomarkers for prognosis and prediction such as tumor size, lymph node status, grade, estrogen receptor positivity, and HER2 expression has led to increased patient overall survival.[53] Additionally, the emergence of novel therapeutics, such as small molecules and immunotherapies, has greatly increased the treatment options to stratified breast cancer patients. However, with the progression of the medical community to a personalized treatment system, the need for useful biomarkers of disease prognosis and treatment is immense.

Histone H1 phosphorylation has long been associated with both DNA relaxation in interphase and the condensation of chromatin during mitosis.[30−36,54−57] However, a recent report suggests that phosphorylation on histone H1 is increased with bladder cancer grade.[8] Furthermore, Telu et al. show the immunohistochemical staining of histone H1 phosphorylation has more specificity than the traditional mitotic stain Ki-67.[8] This report showed convincing in vitro and in vivo data in support of the use of histone H1 phosphorylation as a biomarker for bladder cancer carcinogenesis. Thus, we sought to extend this hypothesis to an additional cancer system. Our data show the utility of histone H1 phosphorylation, specifically at threonine 146, to distinguish between breast cell lines, immortalized breast epithelial MCF-10A, the neoplastic MCF-7, and the metastatic MDA-MB-231 cell lines. More importantly, the pT146 antisera uniquely stain primary tumors with staining intensity associated with tumor grade.

Equally as important as clinical biomarkers, the monitoring of proliferation and therapeutic response is critical to patient care. Such information would allow clinicians to increase, reduce, or stop a dose as therapeutically necessary. Our data show global histone H1 phosphorylation changes in response to extracellular estradiol stimulation and therapeutic LY294002 intervention in in vitro breast cancer models. These data are directly applicable to the clinical monitoring of patient response to antineoplastic agents.

The results presented here establish the need for future study of histone H1 phosphorylation in additional in vivo cancer models to determine the utility as a ubiquitous biomarker of proliferating cells. These data support previous claims that histone H1 could be used in labeling cancer cells and tissues with staining patterns correlating with established clinical stratifications.[7,8] The generation of variant specific immune reagents and the development of more sensitive high specificity assays for pT146, such as multiple reaction monitoring assays, is needed to determine the contribution of the specific H1 isoforms to tumor staining patterns. Such assays, when applied to in vivo samples, hold the potential for further correlation with clinical parameters.

## ASSOCIATED CONTENT

### Supporting Information

Additional information as discussed in text. This material is available free of charge via the Internet at http://pubs.acs.org.

## AUTHOR INFORMATION


### Corresponding Author

*E-mail: freitas.5@osu.edu. Phone: (614) 688-8432. Fax: (614) 688-8675.

### Author Contributions

¶S.W.H. and M.E.H. contributed equally to this work.


### Notes

The authors declare no competing financial interest.

## ACKNOWLEDGMENTS

This work was supported by the NIH/National Cancer Institute (CA154200), Stefanie Spielman Foundation for Breast Cancer Research, and the Anne M. Wolf Breast Cancer Foundation.

## REFERENCES


(1) *Cancer Facts & Figures*; American Cancer Society, 2011; pp 1−68.

(2) Fletcher, S. W.; Elmore, J. G. Mammographic screening for breast cancer. *N. Engl. J. Med.* **2003**, *348*, 1672−1680.

(3) Seligson, D. B.; Horvath, S.; McBrian, M. A.; Mah, V.; Yu, H.; Tze, S.; Wang, Q.; Chia, D.; Goodglick, L.; Kurdistani, S. K. Global levels of histone modifications predict prognosis in different cancers. *Am. J. Pathol.* **2009**, *174*, 1619−1628.

(4) Elsheikh, S. E.; Green, A. R.; Rakha, E. A.; Powe, D. G.; Ahmed, R. A.; Collins, H. M.; Soria, D.; Garibaldi, J. M.; Paish, C. E.; Ammar, A. A.; et al. Global histone modifications in breast cancer correlate with tumor phenotypes, prognostic factors, and patient outcome. *Cancer Res.* **2009**, *69*, 3802−3809.

(5) Manuyakorn, A.; Paulus, R.; Farrell, J.; Dawson, N. A.; Tze, S.; Cheung-Lau, G.; Hines, O. J.; Reber, H.; Seligson, D. B.; Horvath, S.; et al. Cellular histone modification patterns predict prognosis and treatment response in resectable pancreatic adenocarcinoma: results from RTOG 9704. *J. Clin. Oncol.* **2010**, *28*, 1358−1365.

(6) Seligson, D. B.; Horvath, S.; Shi, T.; Yu, H.; Tze, S.; Grunstein, M.; Kurdistani, S. K. Global histone modification patterns predict risk of prostate cancer recurrence. *Nature* **2005**, *435*, 1262−1266.

(7) Burstein, D. E.; Oami, S.; Dembitzer, F.; Chu, C.; Cernaianu, G.; Leytin, A.; Misilim, E.; Jammula, S. R.; Strauchen, J.; Kohtz, D. S. Monoclonal antibody specific for histone H1 phosphorylated by cyclin-dependent kinases: a novel immunohistochemical probe of proliferation and neoplasia. *Mod. Pathol.* **2002**, *15*, 705−711.

(8) Telu, K. H.; Abbaoui, B.; Thomas-Ahner, J. M.; Zynger, D. L.; Clinton, S. K.; Freitas, M. A.; Mortazavi, A. Alterations of histone H1 phosphorylation during bladder carcinogenesis. *J. Proteome Res.* **2013**, *12*, 3317−3326.

(9) Soule, H. D.; Vazguez, J.; Long, A.; Albert, S.; Brennan, M. A human cell line from a pleural effusion derived from a breast carcinoma. *J. Natl. Cancer Inst.* **1973**, *51*, 1409−1416.

(10) Fogh, J.; Trempe, G. New human tumor cell lines. *Human Tumor Cells in Vitro*; Plenum Press: New York, 1975; pp 115−159.

(11) Soule, H. D.; Maloney, T. M.; Wolman, S. R.; Peterson, W. D.; Brenz, R.; McGrath, C. M.; Russo, J.; Pauley, R. J.; Jones, R. F.; Brooks, S. C. Isolation and characterization of a spontaneously immortalized human breast epithelial cell line, MCF-10. *Cancer Res.* **1990**, *50*, 6075−6086.
(12) Bostock, C. J.; Prescott, D. M.; Kirkpatrick, J. B. An evaluation of the double thymidine block for synchronizing mammalian cells at the G1-S border. *Exp. Cell Res.* **1971**, *68*, 163−168.
(13) Ren, C.; Zhang, L.; Freitas, M. A.; Ghoshal, K.; Parthun, M. R.; Jacob, S. T. Peptide mass mapping of acetylated isoforms of histone H4 from mouse lymphosarcoma cells treated with histone deacetylase (HDACs) inhibitors. *J. Am. Soc. Mass Spectrom.* **2005**, *16*, 1641−1653.
(14) Lindner, H.; Sarg, B.; Helliger, W. Application of hydrophilic-interaction liquid chromatography to the separation of phosphorylated H1 histones. *J. Chromatogr. A* **1997**, *782*, 55−62.
(15) Wang, L.; Harshman, S. W.; Liu, S.; Ren, C.; Xu, H.; Sallans, L.; Grever, M.; Byrd, J. C.; Marcucci, G.; Freitas, M. A. Assaying pharmacodynamic endpoints with targeted therapy: flavopiridol and 17AAG induced dephosphorylation of histone H1.5 in acute myeloid leukemia. *Proteomics* **2010**, *10*, 4281−4292.
(16) Su, X.; Jacob, N. K.; Amunugama, R.; Lucas, D. M.; Knapp, A. R.; Ren, C.; Davis, M. E.; Marcucci, G.; Parthun, M. R.; Byrd, J. C.; et al. Liquid chromatography mass spectrometry profiling of histones. *J. Chromatogr. B: Anal. Technol. Biomed. Life Sci.* **2007**, *850*, 440−454.
(17) Bradford, M. M. A rapid and sensitive method for the quantitation of microgram quantities of protein utilizing the principle of protein-dye binding. *Anal. Biochem.* **1976**, *72*, 248−254.
(18) Garcia, B. A.; Busby, S. A.; Barber, C. M.; Shabanowitz, J.; Allis, C. D.; Hunt, D. F. Characterization of phosphorylation sites on histone H1 isoforms by tandem mass spectrometry. *J. Proteome Res.* **2004**, *3*, 1219−1227.
(19) Whitfield, M. L.; Sherlock, G.; Saldanha, A. J.; Murray, J. I.; Ball, C. A.; Alexander, K. E.; Matese, J. C.; Perou, C. M.; Hurt, M. M.; Brown, P. O.; et al. Identification of genes periodically expressed in the human cell cycle and their expression in tumors. *Mol. Biol. Cell* **2002**, *13*, 1977−2000.
(20) Team, R. C. *R: A Language and Environment for Statistical Computing*; R Foundation for Statistical Computing: Vienna, Austria, 2012.
(21) Meyer, D.; Zeileis, A.; Hornik, K. The Strucplot framework: visualizing multi-way contingency tables with vcd. *J. Stat. Software* **2006**, *17*, 1−48.
(22) Meyer, D.; Zeileis, A.; Hornik, K. *vcd: Visualizing Categorical Data*, 2013.
(23) Zeileis, A.; Meyer, D.; Hornik, K. Residual-based shadings for visualizing (conditional) independence. *J. Comput. Graph. Stat.* **2007**, *16*, 507−525.
(24) Sarg, B.; Helliger, W.; Talasz, H.; Förg, B.; Lindner, H. H. Histone H1 phosphorylation occurs site-specifically during interphase and mitosis: identification of a novel phosphorylation site on histone H1. *J. Biol. Chem.* **2006**, *281*, 6573−6580.
(25) Zheng, Y.; John, S.; Pesavento, J. J.; Schultz-Norton, J. R.; Schiltz, R. L.; Baek, S.; Nardulli, A. M.; Hager, G. L.; Kelleher, N. L.; Mizzen, C. A. Histone H1 phosphorylation is associated with transcription by RNA polymerases I and II. *J. Cell Biol.* **2010**, *189*, 407−415.
(26) Harshman, S. W.; Chen, M. M.; Branson, O. E.; Jacob, N. K.; Johnson, A. J.; Byrd, J. C.; Freitas, M. A. Isolation and analysis of linker histones across cellular compartments. *J. Proteomics* **2013**, *91*, 595−604.
(27) Harshman, S. W.; Young, N. L.; Parthun, M. R.; Freitas, M. A. H1 histones: current perspectives and challenges. *Nucleic Acids Res.* **2013**, *41*, 9593−9609.
(28) Garcia, B. A.; Mollah, S.; Ueberheide, B. M.; Busby, S. A.; Muratore, T. L.; Shabanowitz, J.; Hunt, D. F. Chemical derivatization of histones for facilitated analysis by mass spectrometry. *Nat. Protoc.* **2007**, *2*, 933−938.
(29) Garcia, B. A.; Joshi, S.; Thomas, C. E.; Chitta, R. K.; Diaz, R. L.; Busby, S. A.; Andrews, P. C.; Ogorzalek Loo, R. R.; Shabanowitz, J.; Kelleher, N. L.; et al. Comprehensive phosphoprotein analysis of linker histone H1 from *Tetrahymena thermophila*. *Mol. Cell. Proteomics* **2006**, *5*, 1593−1609.
(30) Bradbury, E. M.; Inglis, R. J.; Matthews, H. R.; Sarner, N. Phosphorylation of very-lysine-rich histone in *Physarum polycephalum*. Correlation with chromosome condensation. *Eur. J. Biochem.* **1973**, *33*, 131−139.
(31) Gurley, L. R.; Walters, R. A.; Tobey, R. A. Sequential phsophorylation of histone subfractions in the Chinese hamster cell cycle. *J. Biol. Chem.* **1975**, *250*, 3936−3944.
(32) Hohmann, P.; Tobey, R. A.; Gurley, L. R. Phosphorylation of distinct regions of f1 histone. Relationship to the cell cycle. *J. Biol. Chem.* **1976**, *251*, 3685−3692.
(33) D'Anna, J. A.; Gurley, L. R.; Deaven, L. L. Dephosphorylation of histones H1 and H3 during the isolation of metaphase chromosomes. *Nucleic Acids Res.* **1978**, *5*, 3195−3208.
(34) Gurley, L. R.; D'Anna, J. A.; Barham, S. S.; Deaven, L. L.; Tobey, R. A. Histone phosphorylation and chromatin structure during mitosis in Chinese hamster cells. *Eur. J. Biochem.* **1978**, *84*, 1−15.
(35) Matsumoto, Y.; Yasuda, H.; Mita, S.; Marunouchi, T.; Yamada, M. Evidence for the involvement of H1 histone phosphorylation in chromosome condensation. *Nature* **1980**, *284*, 181−183.
(36) Ajiro, K.; Borun, T. W.; Cohen, L. H. Phosphorylation states of different histone 1 subtypes and their relationship to chromatin functions during the HeLa S-3 cell cycle. *Biochemistry* **1981**, *20*, 1445−1454.
(37) Wiśniewski, J. R.; Zougman, A.; Krüger, S.; Mann, M. Mass spectrometric mapping of linker histone H1 variants reveals multiple acetylations, methylations, and phosphorylation as well as differences between cell culture and tissue. *Mol. Cell. Proteomics* **2007**, *6*, 72−87.
(38) Wang, B.; Malik, R.; Nigg, E. A.; Körner, R. Evaluation of the low-specificity protease elastase for large-scale phosphoproteome analysis. *Anal. Chem.* **2008**, *80*, 9526−9533.
(39) Olsen, J. V.; Blagoev, B.; Gnad, F.; Macek, B.; Kumar, C.; Mortensen, P.; Mann, M. Global, in vivo, and site-specific phosphorylation dynamics in signaling networks. *Cell* **2006**, *127*, 635−648.
(40) Carrascal, M.; Ovelleiro, D.; Casas, V.; Gay, M.; Abian, J. Phosphorylation analysis of primary human T lymphocytes using sequential IMAC and titanium oxide enrichment. *J. Proteome Res.* **2008**, *7*, 5167−5176.
(41) Hergeth, S. P.; Dundr, M.; Tropberger, P.; Zee, B. M.; Garcia, B. A.; Daujat, S.; Schneider, R. Isoform-specific phosphorylation of human linker histone H1.4 in mitosis by the kinase Aurora B. *J. Cell Sci.* **2011**, *124*, 1623−1628.
(42) Talasz, H.; Sarg, B.; Lindner, H. H. Site-specifically phosphorylated forms of H1.5 and H1.2 localized at distinct regions of the nucleus are related to different processes during the cell cycle. *Chromosoma* **2009**, *118*, 693−709.
(43) Majewski, I. J.; Bernards, R. Taming the dragon: genomic biomarkers to individualize the treatment of cancer. *Nat. Med.* **2011**, *17*, 304−312.
(44) Renoir, J.-M.; Marsaud, V.; Lazennec, G. Estrogen receptor signaling as a target for novel breast cancer therapeutics. *Biochem. Pharmacol.* **2013**, *85*, 449−465.
(45) An, J.; Tzagarakis-Foster, C.; Scharschmidt, T. C.; Lomri, N.; Leitman, D. C. Estrogen receptor beta-selective transcriptional activity and recruitment of coregulators by phytoestrogens. *J. Biol. Chem.* **2001**, *276*, 17808−17814.
(46) Oesterreich, S.; Zhang, P.; Guler, R. L.; Sun, X.; Curran, E. M.; Welshons, W. V.; Osborne, C. K.; Lee, A. V. Re-expression of estrogen receptor alpha in estrogen receptor alpha-negative MCF-7 cells restores both estrogen and insulin-like growth factor-mediated signaling and growth. *Cancer Res.* **2001**, *61*, 5771−5777.
(47) Paruthiyil, S.; Parmar, H.; Kerekatte, V.; Cunha, G. R.; Firestone, G. L.; Leitman, D. C. Estrogen receptor beta inhibits human breast cancer cell proliferation and tumor formation by causing a G2 cell cycle arrest. *Cancer Res.* **2004**, *64*, 423−428.

(48) Zhang, J.; Yang, P. L.; Gray, N. S. Targeting cancer with small molecule kinase inhibitors. *Nat. Rev. Cancer* **2009**, *9*, 28−39.
(49) Zheng, X.; Jiang, F.; Katakowski, M.; Zhang, Z. G.; Lu, Q.-E.; Chopp, M. ADAM17 promotes breast cancer cell malignant phenotype through EGFR-PI3K-AKT activation. *Cancer Biol. Ther.* **2009**, *8*, 1045−1054.
(50) Sliva, D.; Rizzo, M. T.; English, D. Phosphatidylinositol 3-kinase and NF-κB regulate motility of invasive MDA-MB-231 human breast cancer cells by the secretion of urokinase-type plasminogen activator. *J. Biol. Chem.* **2002**, *277*, 3150−3157.
(51) Hudis, C. A.; Gianni, L. Triple-negative breast cancer: an unmet medical need. *Oncologist* **2011**, *16*, 1−11.
(52) Foulkes, W. D.; Smith, I. E.; Reis-Filho, J. S. Triple-negative breast cancer. *N. Engl. J. Med.* **2010**, *363*, 1938−1948.
(53) Weigel, M. T.; Dowsett, M. Current and emerging biomarkers in breast cancer: prognosis and prediction. *Endocr.-Relat. Cancer* **2010**, *17*, R245−R262.
(54) Taylor, W. R.; Chadee, D. N.; Allis, C. D.; Wright, J. A.; Davie, J. R. Fibroblasts transformed by combinations of ras, myc and mutant p53 exhibit increased phosphorylation of histone H1 that is independent of metastatic potential. *FEBS Lett.* **1995**, *377*, 51−53.
(55) Chadee, D. N.; Taylor, W. R.; Hurta, R. A.; Allis, C. D.; Wright, J. A.; Davie, J. R. Increased phosphorylation of histone H1 in mouse fibroblasts transformed with oncogenes or constitutively active mitogen-activated protein kinase kinase. *J. Biol. Chem.* **1995**, *270*, 20098−20105.
(56) Herrera, R. E.; Chen, F.; Weinberg, R. A. Increased histone H1 phosphorylation and relaxed chromatin structure in Rb-deficient fibroblasts. *Proc. Natl. Acad. Sci. U.S.A.* **1996**, *93*, 11510−11515.
(57) Chadee, D. N.; Allis, C. D.; Wright, J. A.; Davie, J. R. Histone H1b phosphorylation is dependent upon ongoing transcription and replication in normal and ras-transformed mouse fibroblasts. *J. Biol. Chem.* **1997**, *272*, 8113−8116.